SENSITIVITY STUDY OF INSTRUMENTED NANOINDENTATION FOR MECHANICAL CHARACTERIZATION OF POLYMERS

Kevin D. Cole[(1)], Joseph A. Turner[(2)] , Matthew Stagemeyer [(2)], Mark R. VanLandingham[(3)]

[(1)]Mechanical Engineering Dept., University of Nebraska, Lincoln, NE 68588-0656, kcole1@unl.edu
[(2)] Engineering Mechanics Dept., University of Nebraska, Lincoln, NE 68588-0526
[(3)] Army Research Laboratory, Aberdeen Proving Ground, MD 21005-5069

ABSTRACT

As part of a broader study of the mechanical properties of polymers, a sensitivity study is carried out on the dynamic models used for instrumented nanoindentation which are used in the interpretation of the experimental data. Properties of PDMS (a rubbery polymer) are found from experimental nanoindentation data in a point-by-point procedure at each frequency, and by whole-domain estimation over multiple frequencies. The estimation results are less affected by noise in the data, but somewhat dependent on the chosen frequency range.

1. NOMENCLATURE

A	= indenter contact area
b	= parameters
c_i	= instrument damping, Ns/m
c_s	= instrument damping, Ns/m
E’	= reduced storage modulus
E’’	= reduced loss modulus
f	= frequency, Hz
F_0	= oscillating force, N
k_i	= instrument stiffness, N/m
k_s	= sample stiffness, N/m
m	= mass
S	= sum of square error
x	= time history of displacement
X	= displacement amplitude
Y	= experimental data
$\hat{Y}$	= model estimate

Greek

φ	= phase of displacement
ω	= frequency, rad/s
χ	= sensitivity coefficient

2. INTRODUCTION

Because of an emphasis on lighter weight and multifunctional materials, polymers and polymer composites (traditional and nanocomposites) play critical roles in many current and future Army applications including blast and impact mitigation (i.e., armor). New polymers and polymer composites, produced in the laboratory in small sample sizes, can be produced much faster than they can be quantitatively characterized. Recent advancements in instrumented nanoindentation have resulted in capabilities for characterizing mechanical behavior in small-sized samples from quasi-static rates to ultrasonic frequencies. Current capabilities for deriving quantitative mechanical properties of polymers from nanoindentation tests are severely limited, because (a) the current dynamic models used to describe the tip-sample interactions only crudely approximate viscoelastic behavior, and (b) current data-analysis practice involves computing parameters at one frequency at a time.

This work reported in this paper is a first step towards better utilization of the data from instrumented nanoindentation measurements on polymers. This paper is divided into several sections. First a brief description is given of the nanoindentation unit and the experimental procedures used to obtain data from a PDMS sample. Then the model used to analyze data is presented, along with the relations used to determine the loss and storage modulus. Experimental data froma PDMS sample is analyzed with the pointwise procedure, one frequency at a time. Next a sensitivity study of the model is given, followed by new results found from a parameter estimation technique applied over a range of frequencies. The paper concludes with a discussion of future work.

3. EQUIPMENT AND PROCEDURES

A schematic of the experimental apparatus for nano-indentation is shown in Figure 1. The nanoindentation instrument makes use of a three-place capacitive transducer capable of providing motion in the vertical direction and can measure both force and displacement simultaneously. Force is applied through electrostatic

actuation while displacement is measured by the change in capacitance. An indenter tip is screwed in place in the transducer. The tip used must have a calibrated area function in order to accurately interpret the measured results. The transducer is mounted on an AFM stand with the sample placed on the piezoelectric scanner.

Before the instrument can be used for measurement, an "air indent" is performed to ensure proper calibration of the transducer and to calculate values for machine stiffness and machine damping. A load function is then coded into the software that controls the instrument. For the present work, with dynamic testing, the load function involved ramping the force up to a desired static value and then a small sinusoidal oscillating force is superposed at a prescribed frequency and amplitude. The experiments conducted for this paper were of variable frequency type, which involved prescribing a maximum load to be reached, and a sinusoidal oscillation about this load at a specific amplitude with the oscillation frequency varying through a desired range. The dynamic testing is capable of returning values for elastic modulus, storage modulus, loss modulus, phase etc.

The experimental data is recorded in a computer file, by software provided with the nanoindenter unit, in the form of a table of values over a range of frequencies. The recorded information includes input values: applied static force; applied oscillatory force; and, oscillation frequency. Recorded output values are the displacement amplitude and displacement phase at each frequency.

3. MODEL

In order to extract the properties of the sample from the experimental data, a suitable model is needed. Figure 2 shows the spring/dashpot model used for interpreting dynamic indentation data. The instrument is represented by a spring, dashpot and mass (properties k_i, c_i, and m_i) and the sample is represented by a spring and dashpot (properties (k_s and c_s). This model of the sample, though elementary, does provide repeatable results for trends in the damping present in polymeric materials.

The dynamic response of the model will be used for interpretation of the experimental data. Specifically, we seek the sinusoidal displacement of the indenter mass when a sinusoidal force is applied. The equation of motion for the indenter mass is given by

$$m\ddot{x} + (c_s + c_i)\dot{x} + (k_s + k_i)x = F_0 \sin \omega t \qquad (1)$$

The solution for displacement, x, may be formally stated

$$x = X \sin(\omega t - \varphi) \qquad (2)$$

The dynamic response is measured through X and φ, the amplitude and phase of the displacement, respectively. The formal analytical solution for the equation of motion, in terms of amplitude and displacement, is given by

$$X = \frac{F_0}{\sqrt{[(k_s + k_i) - m\omega^2]^2 + (c_s + c_i)^2 \omega^2}} \qquad (3)$$

$$\varphi = \tan^{-1}\left(\frac{(c_s + c_i)\omega}{(k_s + k_i) - m\omega^2} \right) \qquad (4)$$

The usual approach is algebraic inversion of the above relationships to solve for the sample values at each frequency [1]. That is,

$$k_s = \frac{F_0}{X}\cos\varphi + m\omega^2 - k_i \qquad (5)$$

$$c_s = \frac{F_0}{X\omega}\sin\varphi - c_i \qquad (6)$$

The sample spring and dashpot constants, k_s and c_s, have been introduced for the purpose of the model. The actual parameters of interest for the sample are the storage modulus and the loss modulus, which can be related to the model values by Hertzian theory for a circular punch in contact with a half space [2]

$$E' = \frac{k_s}{2}\sqrt{\frac{\pi}{A}}; \quad E'' = \frac{\omega c_s}{2}\sqrt{\frac{\pi}{A}} \qquad (7)$$

Here A is the contact area and E' and E'' are the reduced storage and loss coefficients, respectively [3].

For most indenters (spherical, Berkovitch, etc.) the contact area must be carefully calibrated as function of displacement depth. For the present work, however, a flat circular punch (diameter 500 micrometers) is used for which the contact area is independent of displacement.

4. DATA ANALYSIS

In this section nanoindentation data is analyzed to obtain mechanical properties. Figure 3 shows experimental data for displacement (amplitude and phase) plotted versus frequency, obtained from a Hysitron nanoindentation unit on a sample of PDMS polymer. A flat circular punch was used as the indenter. Note that the experimental data is quite smooth over the range of frequencies studied.

If the instrument parameters are known (or found from calibration), then the above relations can be used to determine the sample properties E' and E''. The calibration data associated with the data are given in

Table 1. Next, two approaches to analysis of the data are discussed.

4.1 Pointwise estimation.

In this approach, data at each frequency (X , φ.) are used to compute sample properties at each frequency. This is the approach used in the software provided by the nanoindenter manufacturer [4].

Figure 4 shows the values of storage and loss modulus obtained by point-by-point application of Eqs. (5-7). The values for E' and E'' vary smoothly with frequency in the middle of the frequency range, but there is some scatter at low frequencies and more scatter in the results at high frequencies. The scatter in the results is non-physical, as we expect gradual and smooth variation in the moduli as a function of frequency. The scatter in the results must therefore be a results of noise in the raw data, even though the raw data does not appear to be "noisy". In some way the data analysis seems so be amplifying a small amount of noise present in the data, and this effect is more pronounced at higher frequencies.

4.2 Whole-domain estimation.

Another approach to analyzing the data is parameter estimation, whereby data from many frequencies is considered together in a regression scheme to find the best fit between the model and the data. For this method, the functional form of the frequency variation of the moduli must be chosen. For simplicity we seek a power law of the form

$$E'(f) = b_1 (f / f_r)^{b_3} \tag{7}$$

$$E''(f) = b_2 \left(f / f_r\right)^{b_3} \tag{8}$$

where f_r is the instrument resonance frequency and the parameters to be sought are b_i , i = 1,2, 3.

Next, let the displacement data at each frequency be denoted $Y(\omega)$ (representing both amplitude and phase information), and let $\hat{Y}(\omega, b_j)$ represent values computed from the model with Eq. (5 – 8) which depend upon parameter values b_j. The level of fit between the data and the model is measured by the sum-of-square error,

$$S = \sum_{i=1}^{N} [Y(\omega) - \hat{Y}(\omega, b_j)]^2 \tag{9}$$

The procedure to determine the best parameters is to minimize S by varying parameters b_j, and then best-fit parameter values represent the best estimates for the sample properties. In this research we use a Levenberg-Marquardt technique to minimize the sum-of-square error [5].

The parameter estimation approach involves the use of sensitivity coefficients, which are derivatives of the model values with respect to the parameters. The sensitivity coefficients are defined by

$$\chi_j = b_j \frac{d\hat{Y}}{db_j} \tag{10}$$

Each derivative is multiplied by the parameter so that the units of χ_j associated with each parameter have the same units, and can be directly compared with one another.

It is important to examine the sensitivity coefficients. In order for a successful fit between data and the model, the sensitivity coefficients should be as large as possible. Further, for two or more parameters to be sought simultaneously, the sensitivity coefficients need to be linearly independent [6]. A careful examination of the sensitivity coefficients can suggest how to adjust the conditions of the experiment in order to improve the data fit which in turn should improve the estimated values of the desired parameters.

Figures 5 and 6 show the sensitivity coefficients plotted versus frequency, computed from the model. Table 1 lists calibration values used in the model along with values b_1 = 0.2 MPa, b_2 = 0.02 MPa, and b_3 = 0 (that is, the moduli were taken to be constant over all frequencies). An important feature of the sensitivity curves shown in Figs. 5 and 6 are that the peak values lie near the resonance of the instrument, at $\sqrt{m_i / k_i}$ =127 Hz. This is where the instrument is most sensitive. In Fig. 5, showing amplitude sensitivity, the values quickly decay towards zero away from resonance. The phase sensitivity, shown in Fig. 6, approaches a non-zero constant at smaller frequencies, unlike that for amplitude sensitivity in Fig. 5. This indicates that phase data is more valuable than amplitude data at lower frequencies.

In both Figs. 5 and 6, sensitivity to E' and E'' have very different shapes. This indicates the important property of linear independence which is essential for simultaneous estimation of multiple parameters b_i. Finally, in both Figs. 5 and 6, the peak sensitivity to E' is further from zero than that for E'' (that is, the absolute value is larger). This suggests that E' will be easier to measure (or can be measured with higher confidence) compared to E''.

As a first step, results are given next for analysis of phase data. Working with phase data simplifies the computer coding, as no input data is needed on amplitude. Further, the sensitivity analysis suggests that phase data contains more useful information, especially at lower frequencies.

A computer code was prepared to combine the phase data shown in Fig. 3, the model calculation given

by Eq. (3-8), and a routine to minimize the sum-of-square error. The following best-fit values were obtained: $b_1 = 0.199$; $b_2 = 0.038$; and, $b_3 = -0.0322$. With these values the storage and loss moduli computed from Eq. (7) and (8) are shown in Fig. 7. These moduli values agree somewhat with the values of the pointwise estimates (Fig. 4) near instrument resonance (127 Hz), however away from this point the shape of the frequency dependence is completely different.

In order to assess how well the parameter fits match the data, it is important to compare the model predictions with the experimental data values. Quantitative comparison can be carried out by an examination of the residuals, the difference between the experimental data (phase in this case) and the model values computed at the best-fit parameter values. (A comparison of the two phase curves themselves is useful only for qualitative observations.) Residuals show exactly where and how well the model matches the experimental data. A desirable result would be residuals that are everywhere small and randomly distributed, representing a good fit between model and experiment.

The residuals, shown in Fig. 8, are near zero in the middle of the frequency range. As frequency becomes smaller, the residuals move away from zero in a very systematic way, which suggests that there is a systematic mismatch between the model and the experiment at low frequency. At large frequency, the residuals also move away from zero, but the variation across frequency is less systematic. Although randomness in the residuals shows that there is noise in the data, it also means that the fit in this region may be as good as possible under the circumstances, because the systematic variations have been described by the model.

The systematic variations in the residuals suggest that the fit could be made better by changing something in the model or in the data. The sensitivities suggest that higher frequencies do not contribute much (sensitivities are small there). Thus, for the next step, the fit was repeated with a subset of the same data, over a smaller range of frequencies. Using experimental data in the range $10 < f < 130$ Hz, the following values were obtained by minimizing the sum-of-square-error: $b_1 = 0.199$; $b_2 = 0.038$; and, $b_3 = +0.5607$. Note that the first two parameters did not change (to three digits), but the third parameter, the exponent in the power law, changed sign. With these parameters the frequency variation of the moduli given by Eq. (7) and (8) is much different than before, as shown in Fig. 9. Now both the storage and loss modulus increase as frequency increases, somewhat similar to that found with the pointwise data analysis (see Fig. 2). The residuals, shown in Fig. 10, are smaller than for the previous data fit. In the range $30 < f < 80$ there is some scatter in the residuals that appears to be random, however the residual values in this range are mostly positive, indicating a remaining bias in this frequency range. Finally, because very strong systematic trends remain in the residuals for the smallest and largest frequencies in Fig. 10, the experimental data does not seem to be well uniformly described by the power-law model even for this subset of the data.

The results of the parameter estimates suggest that the power law variation of the moduli is useful over the lower frequencies, but may be inadequate for the whole range of frequency data available. At larger frequencies, something else is going on that the power law does not describe. However at this point in the project it is not clear whether some other model is needed, or whether the sensitivity of the instrument is inadequate at frequencies above instrument resonance. Certainly further work is needed.

5. FUTURE WORK

Future work will include a study including both amplitude and phase data in the parameter fit. Work is also underway to construct a more detailed physical model, based on theory for a rigid indenter oscillating on a viscoelastic halfspace. Such a model may explain more of the frequency dependence seen in the data.

6. CONCLUSION

In this paper a sensitivity analysis is carried out for nanoindentation measurements. The sensitivity coefficients can suggest what range of frequencies are most useful, and whether or not multiple parameters can be estimated from the data. Examination of the residuals provides information about the quality of the parameter fit and can suggest ways to improve the fitting procedure.

This paper is a report on work in progress. Whole-domain parameter estimation was carried out for a power-law variation of the storage and loss modulus with frequency. Data analysis for all the data, and for a subset of the data, gave different trends for the variation of modulus versus frequency, and it is not clear which is most useful. Additional work is needed.

Although parameter estimation provides additional tools for exploring experimental data, it also requires additional choices to be made. These choices, such as choosing which range of data to analyze, must be made on the basis of previous experience. Advances in data analysis can only augment, and never replace, the studied judgement of the experimentalist.

ACKNOWLEDGEMENT

The authors would like to thank the Army Research Laboratory for support of this project.

4. REFERENCES

1. S. A. S. Asif, K. J. Wahl, and R. J. Coulton, Nanoindentation and contact stiffness measurement using force modulation with a capacitive load-displacement transducer, Review of Scientific Instruments, v. 70, no. 5, pp. 2408-2413 (1999).
2. R. J Roark and W. C. Young, Formulas for Stress and Strain, Mcgraw-Hill, , 1975, p. 519.
3. K. L. Johnson, *Contact Mechanics*, Cambridge University Press, 1985, p. 92.
4. Triboscope Users Manual, Hysitron, Inc. Minneapolis, MN (2004).
5. W. H. Press et al, *Numerical Recipes*, Cambridge University Press, 1992, p. 678.
6. J. V. Beck and K. J. Arnold, *Parameter Estimation in Engineering and Science*, Wiley, 1986, p. 349.

Table 1. Calibration data from the nanoindentation experiment.

symbol	value
k_i	331.31 N/m
c_i	0.0595 Ns/m
m_i	0.0005219 kg
A	1.96 (10^{-7}) m^2
F_o	5.45 (10^{-6}) N

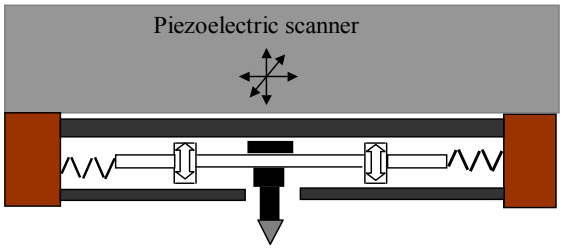

Figure 1. Schematic of nanoindenter with indenter tip mounted on springs inside a capacitive transducer, all mounted on a piezoelectric stage.

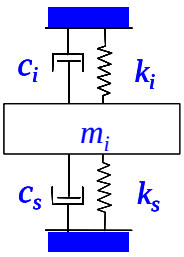

Fig. 2. Spring-dashpot model of instrument (parameters k_i, c_i, m_i) and sample (parameters c_s and k_s).

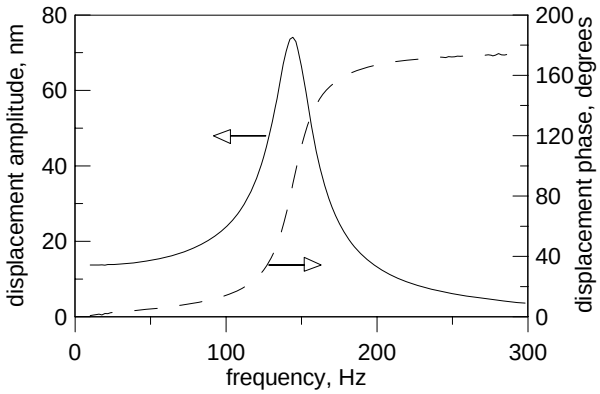

Fig. 3. Amplitude and phase of displacement measured on a PDMS (rubbery polymer) sample with the instrumented nanoindenter unit using a flat punch indenter (data file 7-22-05-1.txt).

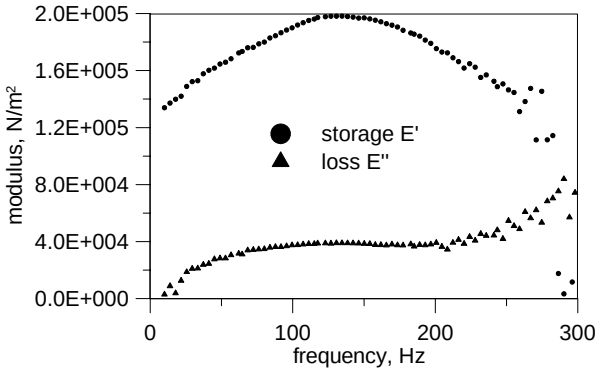

Fig. 4 Storage modulus E' and loss modulus E'' for the PDMS sample interpreted from a point-by-point analysis of the nanonindenter data.

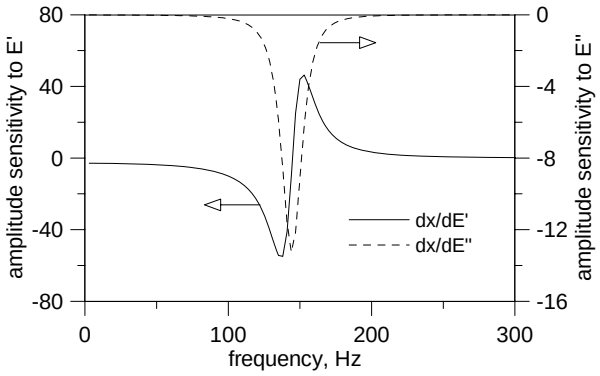

Fig. 5 Amplitude of the sensitivity coefficient with respect to changes in the storage modulus E' and the and loss modulus E''.

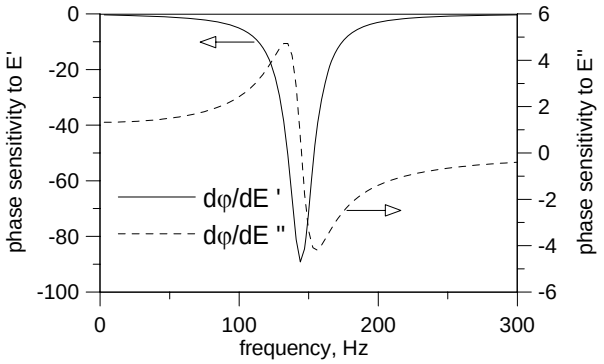

Fig. 6. Phase of the sensitivity coefficient with respect to changes in the storage modulus E' and the and loss modulus E''.

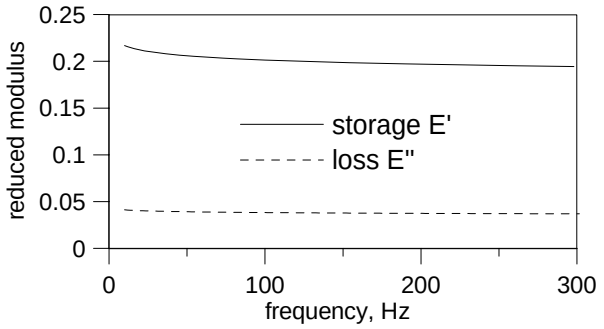

Fig. 7. Power-law variation of the storage modulus E' and the loss modulus E'' found from a best fit between the model and all the experimental data (10 < f < 300 Hz). Only phase data was included in the data fit.

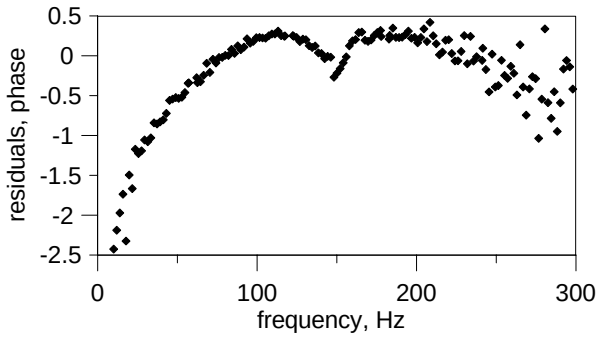

Fig. 8. Residuals (errors between data and model) based on phase information only for the same conditions shown in Fig.7.

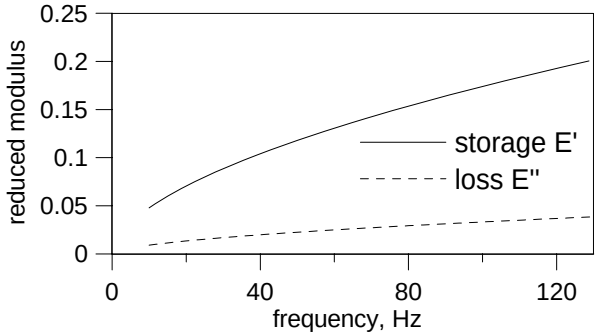

Fig. 9. Power-law variation of the storage modulus E' and the loss modulus E'' found from a best fit between the model and a subset of the experimental data (10 < f < 130 Hz). Only phase data was included in the data fit.

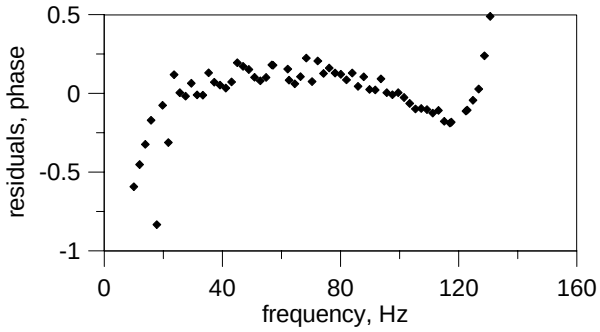

Fig. 10. Residuals (errors between data and model) based on phase information only for the same conditions shown in Fig.9.